Available online at www.sciencedirect.com
ScienceDirect
Journal of Nuclear Materials 360 (2007) 242–254
journal of nuclear materials
www.elsevier.com/locate/jnucmat

Thermodynamic evaluation of the Nb–O–Zr system

R. Jerlerud Pérez [a], A.R. Massih [b,c,*]

[a] Royal Institute of Technology, SE-10044 Stockholm, Sweden
[b] Quantum Technologies, Uppsala Science Park, SE-751 83 Uppsala, Sweden
[c] Malmö University, SE-20506 Malmö, Sweden

Received 15 March 2006; accepted 13 October 2006

Abstract

Thermodynamic properties of the ternary system Nb–O–Zr have been evaluated by means of the CALPHAD (CALculation of PHAse Diagrams) method. The pertinent experimental data are surveyed and the thermodynamic models based on the previous assessments of the binary systems Nb–O, Nb–Zr and O–Zr are delineated. The results of our computations indicate that the models describe the zirconium rich portion of the ternary phase diagram satisfactorily, however, in the niobium rich part, the calculations differ from the experimental data and should be verified by new experiments.

1. Introduction

The Nb–O–Zr system constitutes the basis of several important alloys. The zirconium rich portion of the system, Zr–Nb based alloys, are employed in water cooled nuclear reactors in fuel and core components. For example, the alloys ZIRLO [1] and M5 [2] are increasingly used as fuel cladding materials in pressurised water reactors, Zr–2.5Nb has been employed as a standard material for the pressure tubes in pressurised heavy water reactors [3,4], and E110 [5] and E635 [6] alloys are utilised in the Russian built VVER and RMBK cores. Improving the performance of these alloys to meet the demands of high exposures requires further optimisation in composition and heat-treatment for which a detailed knowledge of the alloy phase equilibria is important.

Alloys, in the niobium rich part of Nb–O–Zr system, e.g., Nb–1Zr based alloys, are leading candidates for components of future space vehicle reactor systems [7,8]; and possibly a suitable material from this family of alloys for the first wall of the future fusion reactors [9,10].

The Nb–O–Zr system has been a subject of several experimental investigations. Asundi et al. [11] have provided a short restricted review of the data up to 1981 and based on that have deduced two ternary phase diagrams for the Nb–O–Zr system at the temperatures 1273 K and 1773 K. Also, it has been referred in the 1999 CALPHAD meeting summary [12] that ternary phase diagrams for the Nb–O–Zr system were assessed and calculated by Dupin and co-workers, however, to best of our knowledge, no publication of this work is yet available in the open literature.

* Corresponding author.
E-mail address: alma@quantumtech.se (A.R. Massih).

0022-3115/$ - see front matter © 2006 Elsevier B.V. All rights reserved.
doi:10.1016/j.jnucmat.2006.10.008

In this paper, we briefly review experimental phase diagram data on the Nb–O–Zr system available in the open literature. The data comprise those reviewed by Asundi et al. plus later studies on this system. Moreover, based on the thermodynamic models and assessed model parameters developed for the binary systems Nb–O [13], Zr–O [14] and Nb–Zr [15], which have been collected in a binary system data base for Zr base alloys [13,16], we calculate the phase diagram of the Nb–O–Zr system at several temperatures of interest and compare the results with measured data. In addition, we compare the calculated solubility of oxygen in this system with measured data.

This paper is organised as follows. In Section 2 a short review of experimental thermochemical data on the Nb–O–Zr system is presented. In Section 3 the ingredients of the thermodynamic modelling is delineated. The results of thermodynamic computations are presented in Section 4. In Section 5, we compare and discuss the computational results with experimental data, which include the oxygen solubility, the energy of formation for niobium oxides and the phase boundaries.

2. Survey of experimental data

In this section a brief review of experimental thermochemical data on the Nb–O–Zr system is made to establish the experimental basis for the verification of the models discussed in the subsequent sections. Table 1 outlines the principal phases which exist in this system, while Table 2 summarizes the range of compositions and temperatures for which measured data are reported in the literature. A more detailed survey is provided in [17].

Zirconium has two allotropic phases, α-Zr (hexagonal close-packed), which is stable up to 1139 K and β-Zr (body-centred cubic). The α-Zr phase dissolves oxygen interstitially and the maximum solubility limit of oxygen in α-Zr is 35 at.% O (8.63 wt%O) at the eutectic temperature of 2338 K [18,14]. Similarly, the β-Zr phase dissolves oxygen interstitially but with the maximum solubility limit of 10.5 at.% O (2.76 wt%O) at 2243 K. Niobium acts as a substitutional element in zirconium. Oxygen stabilises the α-Zr phase, whereas niobium stabilises the β-Zr phase. This difference in phase stability results in a very small solubility limit of oxygen in Zr–Nb alloys despite the fact that solubility limits are very large in β-Nb (bcc), α-Zr and β-Zr.

Niobium has a bcc crystal structure with a melting point of 2741 K and a boiling point of 5015 K. Introduction of oxygen into niobium lowers the melting point to 2188 K at around 10 at.% O. Niobium can also exist in metastable states in the α (hcp) phase [19].

Table 2
Summary of the range of compositions and temperatures studied in phase equilibria experiments made on the Nb–O–Zr system

Zr content (at.%)	O content (at.%)	Temperature (K)	Source
7.5–68	7–61	1773	[29]
1–15	0–5	1273–1473	[25]
0.7–14	0.3–30	1573	[26]
20–25	0.02–0.86	1273–1473	[49]
0–100	0–20	1273&1873	[27]
94–99	0.8–3.0	1197–1457	[20]
2–5.4	0–2.5	293&1173	[56]
2–5	0.02–0.25	1783–2175	[28]
0.33–1.0	66.67	450–1140	[30]
95.5–100	17–28	325–905	[36]
97–99	0.54–2.44	900–1265	[24]

2.1. Zirconium rich region

In the Zr-rich part of the Nb–O–Zr system (0.5–5.6 at.% Nb), Hunt and Niessen [20] have studied

Table 1
Principal phases in binary systems Nb–O, Nb–Zr and O–Zr

Phase name	Composition	Symmetry	Space group
α	(Zr, Nb),(Zr, O),(Zr, Nb, O)	hcp	$P6_3/mmc$
β	As above + (Nb,O)	bcc	$Im\bar{3}m$
α-ZrO_2	ZrO_2	Monoclinic	$P2_1/c$
β-ZrO_2	ZrO_2	Tetragonal	$P4_2/nmc$
γ-ZrO_2	ZrO_{2-x}	Cubic	$Fm\bar{3}m$
NbO	NbO	Cubic	$Pm\bar{3}m$
NbO_2	NbO_2	Tetragonal	$P4_2/mnm$
NbO_2	NbO_2	Distorted tetragonal	$I4_1/a$
β-Nb_2O_5	Nb_2O_{5-x}	Monoclinic	P2
γ-Nb_2O_5	Nb_2O_5	Orthorhombic	Pba2

the effect of oxygen on the equilibrium $\beta \rightarrow (\alpha + \beta)$ transition temperature of Zr–Nb alloys employing quantitative metallography. Their data show a strong impact of oxygen content on the transition temperature, i.e., increasing the oxygen content increases the transition temperature, while there is a weak dependence of the transition temperature on niobium content in the studied range of concentrations. The transition temperature versus oxygen concentration fits an Arrhenius form relation, $X_O = A \exp(-Q/T_t)$, where X_O is the oxygen content, T_t the transition temperature, $A = 4003.96$ (at.%) and $Q = 10352.9$ (K). The actual raw data summarised by Hunt and Niessen [20,21] are listed in Table 3 (translated to units of at.% and kelvin) for convenience.

The equilibrium $\alpha/(\alpha + \beta)$ boundary (temperature versus Nb concentration) in an industrial zirconium alloy containing 2.7 wt%Nb with 0.137 wt%O and 0.09 wt%Fe were determined by Bethune and Williams [22] using electronprobe microanalysis. They found that the solubility limit of the niobium in α-Zr at 873 K is (1.1 ± 0.1) wt%. Later Northwood and Gillies [23] re-determined the $\alpha/(\alpha + \beta)$ and $(\alpha + \beta)/\beta$ boundaries of a single Zr alloy, containing 2.5 wt%Nb with 0.123 wt%O and 0.0545 wt%Fe, using image analysis combined with X-ray determination of α- and β-phases. Their results show that the maximum solubility limit for niobium in the alloy is 0.8 wt% and the monotectoid composition is just about 21 wt%. Moreover, they observed that oxygen raises the transition temperature of α-Zr, while iron is segregated in β-Zr.

More recently, Toffolon et al. [24] examined the influence of oxygen content on $\alpha/(\alpha + \beta)$ and $(\alpha + \beta)/\beta$ transition temperatures in Zr–1 wt%Nb employing calorimetry. Their data indicate that increasing the oxygen content, from about 0.1 wt% to 0.27 wt%, will increase the $(\alpha + \beta)/\beta$ transition temperature from 1185 K to 1265 K, while the $\alpha/(\alpha + \beta)$ temperature varies in the range of 900–910 K. They also studied the influence of niobium content in the range of 0.5–2.5 wt% in Zr alloys containing 0.12–0.13 wt% oxygen. They observed that raising the niobium content lowers both the $(\alpha + \beta)/\beta$ temperature (by about 15 K) and the $\alpha/(\alpha + \beta)$ transition temperature, where the latter remains constant for Nb contents $\geqslant 1$ wt%.

Table 3
The data of Hunt and Niessen [20,21] on the $\beta \rightarrow \alpha + \beta$-phase transition of Zr–Nb–O alloys

O content (at.%)	Nb content (at.%)	Zr content (at.%)	Temperature (K)
0.80	0.50	98.70	1233
0.82	2.38	96.80	1247
0.82	5.56	93.62	1197
1.55	0.50	97.94	1315
1.55	2.52	95.92	1308
1.63	4.27	94.10	1309
3.09	0.51	96.40	1457
2.96	2.30	94.74	1437
3.00	3.93	93.07	1430

2.2. Niobium rich region

The solubility of oxygen in the Nb-rich part of the Nb–Zr system has been a subject of several experimental studies [25–27], for zirconium concentrations in the range of 1–15 at.%, where metallographic and X-ray diffraction techniques have been employed. These studies indicate that the oxygen solid solubility is less than 0.1 at.% O at 1273 K. Marcotte and Larsen [25] using standard vacuum-fusion techniques measured oxygen in Nb–Zr–O alloys at temperatures 1273 K, 1473 K and 1773 K. They found that the solubility of oxygen in niobium-base alloys containing up to 15 at.% Zr is less than 180 wppm.

The solubility of oxygen in the Nb-rich part of the Nb–Zr system has been determined by Jehn and Ortali [28] using a quantitative metallographic technique. Their data, indicate the relation $X_O = A \exp(-Q/T) X_{Zr}^{-1/2}$, where X_O is the solid solubility of oxygen, X_{Zr} is the content of Zr, both in at.%, $A = 2630.27$, $Q = 19\,525.92$ K and T is the absolute temperature. This relation is valid in the temperature range of 1673–2173 K and the composition range of 2–5 at% Zr (where measurements were made). Their data show that the oxygen solubility is lower in the Nb-rich alloys than in the Zr-rich alloys.

Wyder and Hoch [29] investigated, inter alia, the isothermal section of the Nb–Zr–O system at 1773 K, in a broad range of compositions, employing X-ray diffraction and metallographic techniques, from which they constructed a phase diagram for this ternary system at 1773 K. Later, Barber and Morton [26] studied the isothermal section of the Nb–O–Zr system at 1273 K. They utilised X-ray diffraction and metallographic methods to examine the phases, the precipitate size and dispersion of compounds in this system. The Nb-rich portion of the system was studied in the composition range

0–10 wt%Zr and 0–10 wt%O_2. Barber and Morton's main finding for this system was that zirconium saliently reduces the solubility of oxygen by forming ZrO_2, e.g., an addition of 1 wt%Zr lowers the solubility of oxygen in niobium at 1273 K from 3800 wppm to less than 100 wppm. They noted that niobium oxide (NbO) forms as angular particles in brittle solid solution matrix and does not precipitate in dispersed form; whereas zirconium dioxide (ZrO_2) at low concentrations precipitate randomly as spherical particles in a ductile solid solution.

Nakai et al. [10] have studied the effect of oxygen (and/or nitrogen) on phase stability of the Nb–Zr alloys above the monotectoid temperature ($T_{\text{mono}} \approx 895$ K) using optical microscopy, X-ray diffraction, electron microscopy and electronprobe microanalysis. They prepared specimens of Nb–10, 20, 40 and 50 wt%Zr for this purpose. They observed that α-Zr and β-Nb + β-Zr phases precipitate preferably in places where comparatively large amounts of oxygen or nitrogen are present, i.e., close to the surfaces of the specimens. They noted that the element oxygen (and/or nitrogen) stabilizes the α phase at temperatures above T_{mono}, and also, these elements expand the miscibility gap (monotectoid loop) of the phase diagram. Nakai et al., however, did not specify the oxygen content of the alloys, hence their results are only qualitative.

Seta and Naito [30] have studied the Nb-rich part of the Nb–O–Zr system, regarding the phase transition temperature of NbO_2. NbO_2 undergoes a phase transition at about 1070 K from a high temperature tetragonal phase to a low temperature distorted tetragonal structure [31]. In particular, employing calorimetry (directed heat-pulse), they measured the heat capacity and the electric conductivity of $Nb_{1-x}Zr_xO_2$ in the range of $x = 0.01$–0.03. It was shown that the transition temperature of this compound decreased linearly with increasing x according to $T_t(x) = T_t(0) - 1700x$, where $T_t(0) = 1074$ K. The change in the transition temperature with mole fraction of Zr suggests that this transition is caused by the change of the cation–cation bond, i.e., the decrease of T_t is due to the number of cation–cation pairs. In $Nb_{1-x}Zr_xO_2$ the valence of each cation is expressed as $(Nb^{4+}_{1-x}Zr^{4+}_x)O_2$. In the low-temperature phase, however, Seta and Naito note that $Nb^{4+}Nb^{4+}$ pairs form and the compound may be represented by $([2Nb^{4+}]_{(1-2x)/2}Nb^{4+}_xZr^{4+})O_2$, where $[2Nb^{4+}]$ denotes the $Nb^{4+}Nb^{4+}$ pair, the concentration of which controls the transition temperature. Seta and Naito also found that the *excess entropy*, due to the phase transition and the electronic heat capacity (cf. [30] for definitions), decreases rapidly with increasing x, which they explained as being due to the change in the electronic structure of the compound. Seta and Naito also measured the lattice parameters of $ZrO_{1-y}Nb_yO_x$ compounds by X-ray diffraction.

2.3. Order–disorder transition

As mentioned earlier, oxygen atoms up to a concentration of 35 at.% O are in solid solution of α-Zr. Oxygen occupies the octahedral interstices of the hcp zirconium lattice, forming ordered structure at higher oxygen compositions. It has been shown by X-ray, electron and neutron diffraction studies that there are three phases of zirconium–oxygen alloys [32–35]: the completely ordered phase α″-Zr, the intra-layer disordered phase α′-Zr, and the completely disordered phase α-Zr.

Tsuji et al. [36] have measured the heat capacities of Zr–O alloys, ZrO_x, for $x = 0.17$, 0.20, 0.28 and 0.31 and those of niobium doped alloys, $(ZrO_{1-y}/Nb_y)O_x$, for $x = 0.17$ and 0.28 and $y = 0.005$ and 0.01, in the temperature range of 325–905 K by an adiabatic scanning calorimeter. They observed two kinds of heat capacity anomalies at two different temperatures in the specimens. The anomaly, at higher temperatures, was attributed to the order–disorder rearrangement of oxygen atoms, while the one, at lower temperatures, was suggested to be a non-equilibrium phenomenon. Based on the heat capacity measurements the transition temperature and the change in enthalpy were determined.

Tsuji et al. [37] have also determined the lattice parameters of $(ZrO_{1-y}/Nb_y)O_x$ (a and c of hexagonal close-packed structure) by means of X-ray diffraction. Their results indicate a slight decrease of the lattice parameters in the range of the Nb contents studied. That is, the impact of variation of y in the range of $y = 0$ to $y = 0.01$ was in the order of fourth decimal (nm scale).

3. Thermodynamic modelling

We utilise the existing thermodynamic models, developed for the various phases of the binary systems, Nb–O, Nb–Zr and O–Zr, for the calculation of the ternary Nb–O–Zr phase diagram. The models comprise the Gibbs energy expressions, obtained by evaluation of experimental data, for

pure elements, substitution solutions, stoichiometric compounds, ordered phases, interstitial solutions, liquid and gas mixtures.

The formalisms of the models have been discussed in many publications and will not be detailed here, see, e.g., Sundman et al. [38] for an overview. The Gibbs energy expressions are input data to the CALPHAD-type software tools used for calculation of phase equilibria/diagrams of compounds. In the CALPHAD (CALculation of PHase Diagrams) methodology one defines the Gibbs energy of each element with respect to its stable magnetically disordered state at 298.15 K and 101 325 Pa, referred to as the stable element reference (SER), as recommended by the Scientific Group Thermodata Europe (SGTE). In the SGTE pure element database [39], the Gibbs energy is expressed in terms of a power series expansion in temperature in the form:

$$G(T) = a + bT + cT\ln(T) + \sum_n d_n T_n, \qquad (1)$$

where n takes the values 2, 3, $-1, \ldots$, and a, b, c, d_n are empirical constants determined by experimental data. The reference states for the pure zirconium, niobium and oxygen are hcp Zr, bcc Nb and gaseous oxygen, respectively.

We have used the Thermo-Calc software [40] and the database for zirconium alloys [17] for thermodynamic analysis of the Nb–O–Zr system. In Thermo-Calc, all the solution phases are described by the sublattice model, which is based on the compound energy formalism [41]. In this framework, e.g., the lattice for a solid state phase can be divided into several sublattices where the fraction of sites at each sublattice can be used as composition parameters [42,43]. For a molten ionic solution, the composition parameters may be divided into two sets, one for cations another for anions, i.e., an ionic solution can be represented by a two-sublattice model. The phase may also be described as substitutional, e.g., the gas phase. We have outlined the basic relations of the compound energy formalism, appropriate to a ternary system, in Appendix A. The computational methodology of Thermo-Calc is well described by Hillert [44] and Jansson [45].

More specifically, for the Nb–O system, we employ the models and expressions of Dupin and Ansara [46,13]. For the Nb–Zr system, the work of Fernandez-Guillermet [15] and for O–Zr the models assessed by Liang et al. [14,13] are utilised. A summary of type of models used here are listed in Tables 4–6, for the Nb–O, Nb–Zr and O–Zr systems, respectively, where a square (□) denotes vacancies. The thermodynamic parameters for the Nb–O system used in our computations are listed in Appendix B.

Table 4
List of models selected for the Nb–O system based on the work of Dupin and Ansara [46,13]

Symmetry	Model	Constitution
Gas	Ideal mixture	$(O, O_2, O_3, Nb, NbO, NbO_2)$
Liquid	Ionic melt	$(Nb^{+2})_P(O^{-2}, \square^{-2}, NbO_2, NbO_{5/2})_Q$
bcc	Interstitial solution	$(Nb)(O, \square)_3$
hcp	Interstitial solution	$(Nb)(O, \square)(\square)$
Cubic NbO	Stoichiometric	$(Nb)(O)$
Tetragonal NbO_2	Stoichiometric	$(Nb)(O)_2$
Monoclinic Nb_2O_5	Stoichiometric	$(Nb)_2(O)_5$

Table 5
List of models selected for the Nb–Zr system, see [15]

Symmetry	Model	Constitution
Liquid	Substitution, Redlich–Kister	(Nb, Zr)
bcc	Substitution, Redlich–Kister	(Nb, Zr)(□)$_3$
hcp	Substitution, Redlich–Kister	(Nb, Zr)(□)(□)

Table 6
List of models selected for the O–Zr system [14,57]

Symmetry	Model	Constitution
Liquid	Ionic melt	$(Zr^{+4})_P(O^{-2}, \square^{-4}, O)_Q$
bcc	Interstitial solution	$(Zr)_1(O, \square)_3$
hcp	Interstitial solution	$(Zr)_1(O, \square)_1$
hcp (α')	Bragg–Williams	$(Zr)_6(O, \square)_2(\square, O)_2(\square, O)_2$
Cubic γ-ZrO_2	Wagner–Schottky	$(Zr)_1(O, \square)_2$
Tetragonal β-ZrO_2	Stoichiometric	$(Zr^{+4})_1(O^{-2})_2$
Monoclinic α-ZrO_2	Stoichiometric	$(Zr^{+4})_1(O^{-2})_2$

4. Thermodynamic calculations

The binary phase diagrams for the Nb–O, O–Zr and Nb–Zr, calculated by using the Thermo-Calc program, equipped with the models delineated in the foregoing section, are presented in Figs. 1–3, respectively. Fig. 1 rests on the unpublished assess-

ment of Dupin and Ansara [46,13]. This assessment shows that the maximum solubility of oxygen in solid Nb at the eutectic temperature of 2192 K is 9 at.%. In this system there exist three types of niobium oxides that melt congruently (Fig. 1).

Fig. 2 shows the stable phases of the O–Zr system based on the assessment of Liang et al. [14]. The maximum solubility of oxygen in β-Zr (bcc phase) is 11.8 at.% O, which occurs at the peritectic temperature of 2241 K. The solid solution of oxygen in α-Zr (hcp phase), on the other hand, has a maximum solubility of 32 at.% and occurs at the eutectic

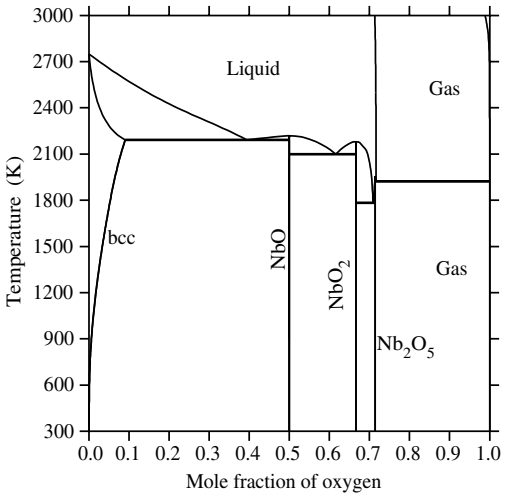

Fig. 1. Calculated phase diagram for the binary Nb–O system using the models outlined in Table 4. The melting temperatures of NbO, NbO_2 and Nb_2O_5 at oxygen contents 0.5, 0.667 and 0.714 (mole fraction) are 2218, 2182 and 1782 (K), respectively.

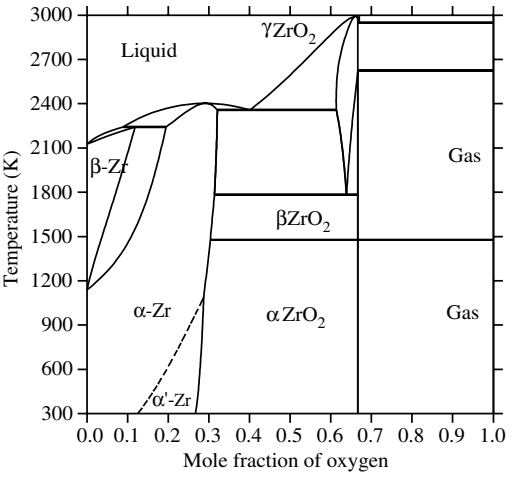

Fig. 2. Calculated phase diagram for the binary O–Zr system using the models outlined in Table 6.

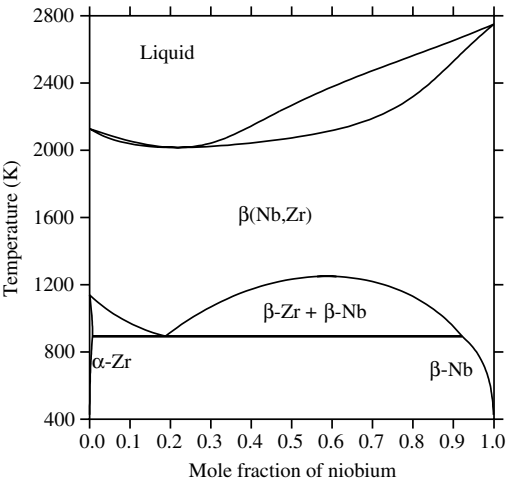

Fig. 3. Calculated phase diagram for the binary Nb–Zr system using the models outlined in Table 5.

temperature of 2357 K. The oxygen atoms occupy the octahedral interstitial sites of the hcp structure, i.e., the octahedral vacancies. At sufficiently high temperatures or low oxygen contents, the oxygen distribution in the sublattice of the octahedral vacancies can be in a disordered state, called α-Zr. This phase is stable up to its congruent melting point of 2400 K at 29 at.% O. At low temperatures there is a phase transition from the disordered phase to an ordered one. The ordered phase is formed by stacking a series of oxygen atom layers parallel to the hcp basal plane in the octahedral vacancies. Below 1270 K, the ordered phase α′-Zr is formed by a second-order transition. As mentioned in

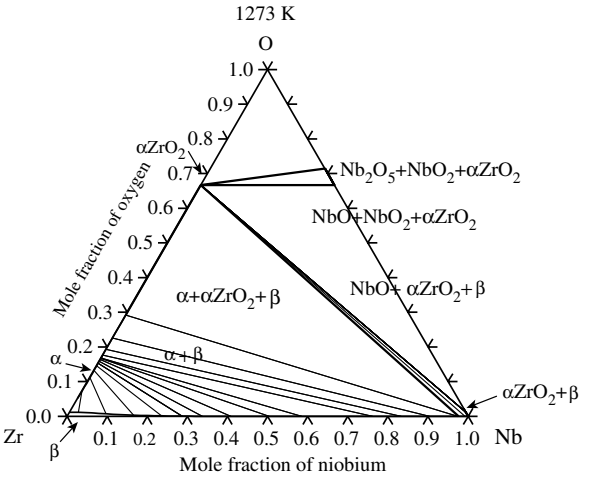

Fig. 4. Calculated isothermal section of the ternary phase diagram for the Nb–O–Zr system at temperature 1273 K.

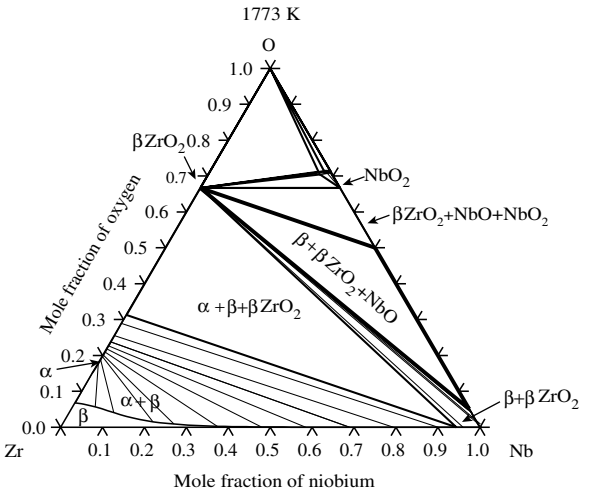

Fig. 5. Calculated isothermal section of the ternary phase diagram for the Nb–O–Zr system at temperature 1773 K.

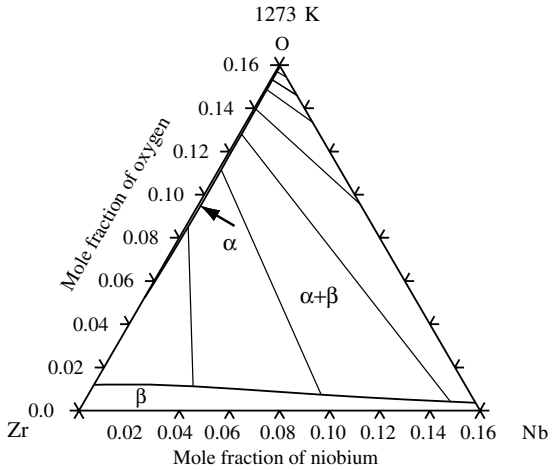

Fig. 6. Calculated isothermal section of the Zr-rich corner of the ternary phase diagram for the Nb–O–Zr system at 1273 K, see Fig. 4.

Section 2, even another ordered hcp phase has been reported α″-Zr [47]. In the Zr–O assessment made by Liang et al. [14], only the ordered α′-Zr has been modelled (Table 6). The order–disorder transition boundary, α-Zr ↔ α′-Zr, is represented by the dashed line shown in Fig. 2. The compound ZrO_2 has three stable modifications: the low temperature stoichiometric compound α-ZrO_2 with monoclinic structure, which is stable up to 1478 K, the tetragonal structure β-ZrO_2, stable up to 2625 K and the non-stoichiometric γ-ZrO_2 with a cubic structure (CaF_2 prototype) and the congruent point at 2995 K.

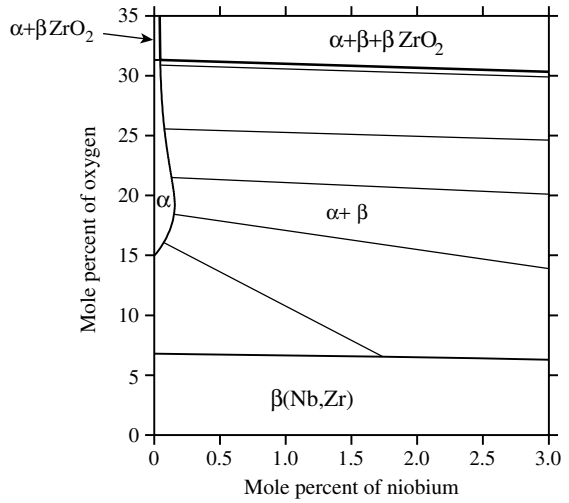

Fig. 7. Calculated isothermal section of the Zr-rich corner of the Nb–O–Zr system at temperature 1773 K, see Fig. 5.

The extrapolation of the binary systems to the ternary system is achieved using the method of Muggianu as described in Ref. [48]. The isothermal sections of the ternary phase diagram at temperatures 1273 and 1773 K are displayed in Figs. 4 and 5, respectively, while Figs. 6 and 7 depict the corresponding diagrams in the Zr-rich corners.

5. Discussion

For the thermodynamic evaluation of the Nb–O–Zr ternary system, we have used the thermodynamic descriptions of the binary systems discussed in the foregoing sections. In order to verify the extrapolation of the assessed binary systems to the ternary system, several isothermal sections were calculated and compared with the available experimental data on the Nb–O–Zr ternary system. The extrapolations are compared with the available experimental data at the Zr-rich corner of the ternary system. In Figs. 8–10 three isothermal sections of the Nb–O–Zr system at 1273 K, 1473 K and 1773 K are presented, respectively. It can be seen that good agreement is reached between the calculated Zr-rich portion of the phase diagram and the experimentally determined two phase field ($\alpha + \beta$, open circles) and the single phase β field (filled circles) of Hunt and Niessen [21] at 1273 and 1473 K. Moreover, the computations are in agreement with the data of Wyder and Hoch [29] at 1773 K. We have also compared the results of our computations of the $\beta \rightarrow (\alpha + \beta)$ transition temperature as a function of niobium

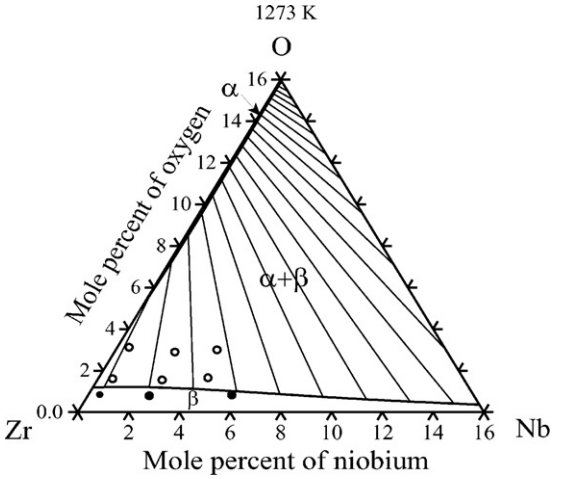

Fig. 8. Calculated isothermal section of the Zr-rich corner of the Nb–O–Zr system at 1273 K and measured data of Hunt and Niessen [21] (open circles: (α + β)-phase region, filled circles: β-phase region).

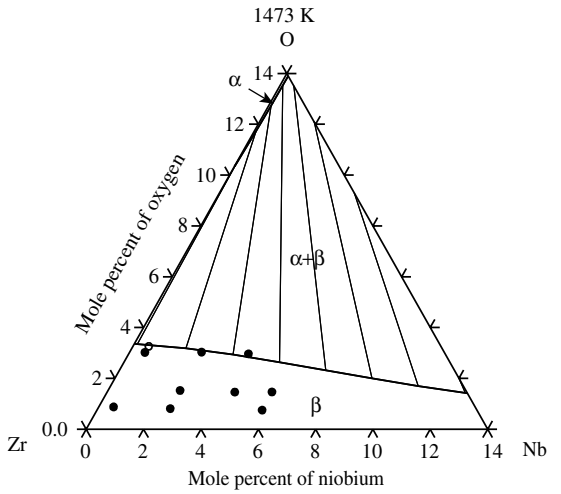

Fig. 9. Calculated isothermal section of the Zr-rich corner of the Nb–O–Zr system at 1473 K and measured data of Hunt and Niessen [21] (open circles: (α + β)-phase region, filled circles: β-phase region).

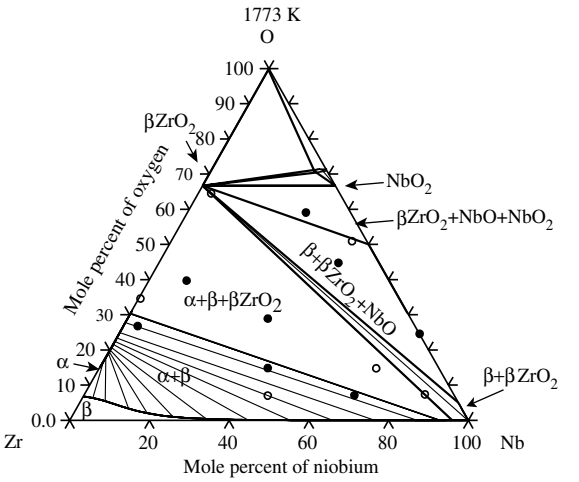

Fig. 10. Calculated isothermal section of the Nb–O–Zr system at temperature 1773 K and measured data of Wyder and Hoch [29] (open circles: two-phase region, filled circles: three-phase region).

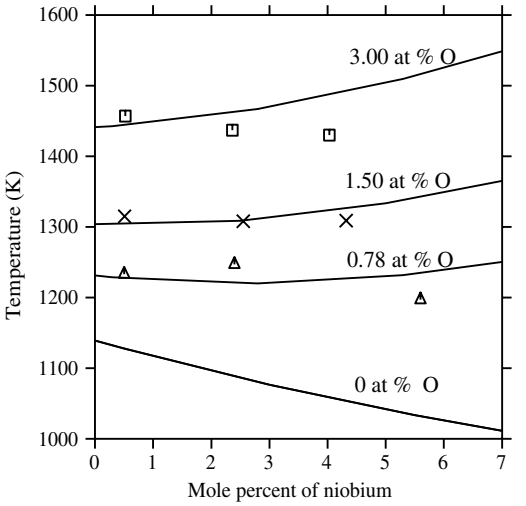

Fig. 11. Calculated versus measured transition temperature $\beta \rightarrow (\beta + \alpha)$ in the Zr-rich portion of the Nb–O–Zr system. Symbols denote measured data at several oxygen contents obtained from [20,21]. The bottom line corresponds to zero oxygen content.

concentration for several oxygen contents with the experimental data of Hunt and Niessen [20,21], Fig. 11.

The calorimetric data of Toffolon et al. [24] on phase transition temperatures in the Zr-rich portion of the Nb–O–Zr system are evaluated using Thermo-Calc with the models alluded in Section 3. The results are presented in Figs. 12 and 13. Fig. 12 shows the isoplethal section of the Nb–O–Zr system with 0.12 wt%O. The symbols denote measured values. For a frame of reference, the same calculation was performed for 1.0×10^{-6} wt%O (grey continuous line), which virtually represents the binary Nb–Zr system. Fig. 13 depicts three isoplethal sections for the Zr-rich portion of this ternary system. The calculations are made for 970 wppm O (black continuous line), 1290 wppm O (dashed line) and 2745 ppm O (grey line) and are compared with the experimental data (symbols) obtained by Toffolon et al. [24] at 0.98 at.% Nb. It is

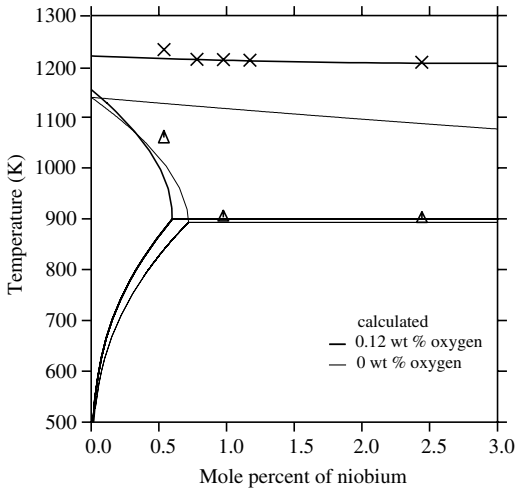

Fig. 12. Calculated isoplethal section of Zr–Nb–0.12 wt%O alloy and measured data of Toffolon et al. [24]. The symbols denote measured data: $\Delta = \alpha \rightarrow (\alpha + \beta)$ temperature; $x = (\alpha + \beta) \rightarrow \beta$ temperature. The lines are calculated by Thermo-Calc: black lines are for 0.12 wt%O and grey lines for 0.0 wt%O (reference frame).

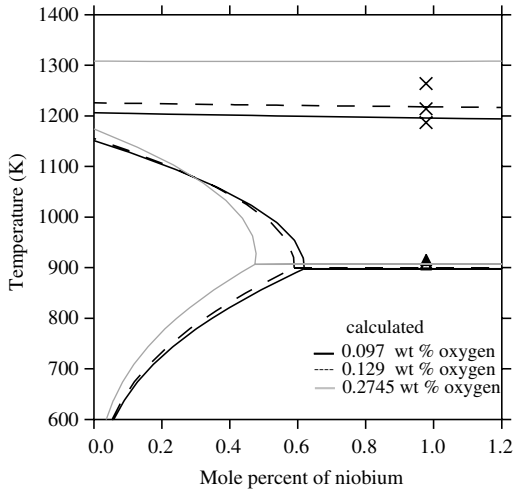

Fig. 13. Calculated isoplethal section of Zr-rich portion of the Zr–O–Nb system and measured data of Toffolon et al. [24]. The symbols denote measured data: $\Delta = \alpha \rightarrow (\alpha + \beta)$ temperature; $x = (\alpha + \beta) \rightarrow \beta$ temperature. The lines are calculated by Thermo-Calc: grey lines are for 0.2745 wt%O, dashed lines for 0.129 wt%O, black lines for 0.097 wt%O.

seen that agreement between calculations and measurements is satisfactory. Hence in general, the model extrapolations from the binaries to the ternary system capture the measured phase boundary $\alpha \leftrightarrow \beta$ adequately.

On the other hand, in the Nb-rich portion of the phase diagram, the binary model extrapolations differ from the accepted ternary diagram. As can be seen from Figs. 14–16, in the isothermal sections at temperatures 1273, 1473, and even at 1773 K, the boundary between the two-phase fields and the tie-triangles does not fit all the experimental results in Refs. [25,26,49]. In Fig. 14 the experimental data on the three-phase triangle $Nb + NbO + ZrO_2$ is well fitted but the two-phase field $Nb + NbO$ does not extend into the ternary because no solubility of Zr has been allowed in NbO.

The calculated two-phase field monoclinic $ZrO_2 + \beta$-Nb region is narrower than that found

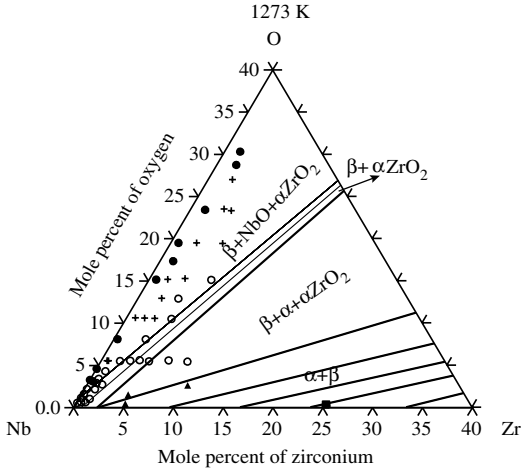

Fig. 14. Calculated isothermal section of the Nb-rich portion of the Nb–O–Zr system at 1273 K. Measured data are from Ref. [26] ($\circ = \beta + ZrO_2$ mono, $\bullet = \beta + NbO$, $+ = \beta + NbO + ZrO_2$ mono), [49] ($\blacktriangle = \alpha + \beta + ZrO_2$ mono) and [25] ($\blacksquare = \beta$).

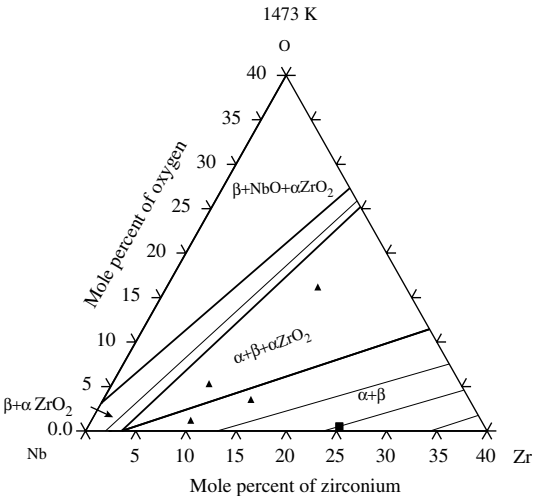

Fig. 15. Calculated isothermal section of the Nb-rich portion of the Nb–O–Zr system at 1473 K. Measured data are from Ref. [25] ($\blacktriangle$ = three-phase region) and [49] ($\blacksquare$ = two-phase region).

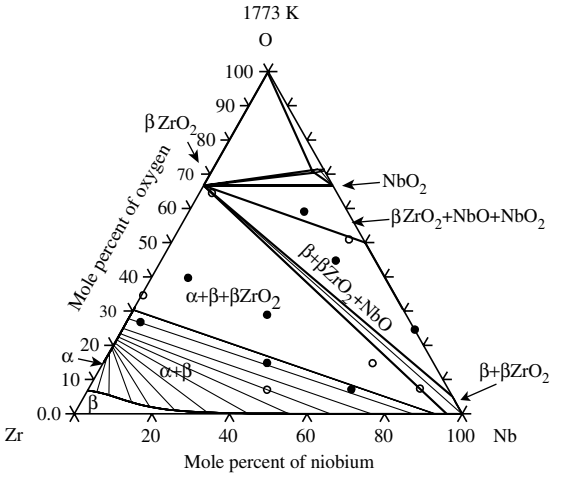

Fig. 16. Calculated isothermal section of the Nb–O–Zr system at 1773 K. Measured data are from [29] (● = three-phase region, ○ = two-phase region).

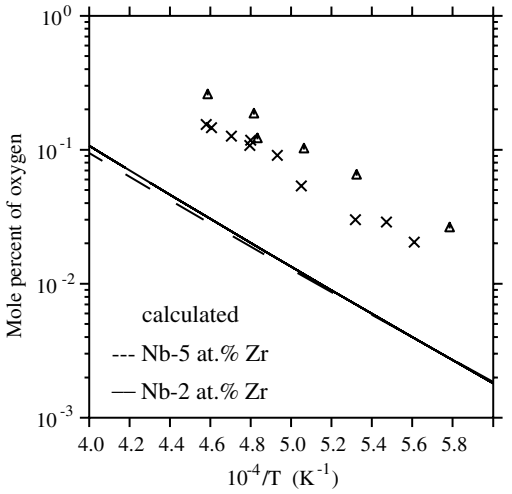

Fig. 17. The oxygen solubility versus reciprocal temperature in Nb–Zr alloys for Nb–5 at.% Zr and Nb–2 at.% Zr (calculated dashed and solid lines) compared with the experimental data (x = Nb–5 at.% Zr, Δ = Nb–2 at.% Zr) by Jehn and Ortali [28].

experimentally by Barber and Morton [26], but the three-phase equilibrium α + monoclinic-ZrO_2 + β-Nb agrees well with the experiments by Marcotte and Larsen [25]. Since the composition of monoclinic ZrO_2 is fixed, the only way to make the two-phase region wider is to increase the content of Zr in β-Nb in the three-phase equilibrium, but that would militate the experiments by Marcotte and Larsen [25].

The calculated solubility of oxygen in β-Nb phase does not agree with some of the experimental data. According to our calculations, oxygen reacts strongly with zirconium to form ZrO_2 and as the zirconium content increases very little oxygen remains in β-Nb. In Refs. [25–28], it was experimentally established that the addition of zirconium drastically would decrease the oxygen solubility in β-Nb. The solubility data reported in Refs. [25,26] are less than 100 wppm (0.05 at.% O) in Nb–1 at.% Zr alloys, for the temperature range of 1273–1473 K, and the solubility limit reported in [27] for Nb–0.4 at.% Zr was 0.025 at.% O at 1273 K. In Fig. 14, the solubility of oxygen in the three-phase equilibrium β-Nb + α + monoclinic-ZrO_2 is very low. At 3 at.% Zr, the α-Zr phase would already form because the oxygen has been rejected from the β-phase.

The computed solubilities of oxygen in Nb–2 at.% Zr and Nb–5 at.% Zr together with the experimental data of Jehn and Ortali [28] are shown in Fig. 17. As can be seen, the trend is predicted correctly but the calculated values are by an order of magnitude lower than the experimental results, and they are even lower than the data reported in Refs. [25–27]. However, it is not clear if the experimental data by [28] really represent the oxygen content in β-Nb or the overall oxygen composition in the two-phase field β-Nb + ZrO_2 at some unknown oxygen potential. In Fig. 18 the Nb-rich corner is plotted with logarithmic composition axes and the decrease of oxygen solubility with increasing zirconium content is a straight line, representing the constant solubility product $x_{Zr}x_O^2$. When the monoclinic ZrO_2 is in equilibrium with Zr in the bcc phase, the energy balance requires

$$ {}^0G^{\text{mono}}_{ZrO_2} = {}^0G^{\text{bcc}}_{Zr} + 2\,{}^0G^{\text{bcc}}_{O}. \tag{2} $$

Here ${}^0G^{\text{bcc}}_{Zr}$ and ${}^0G^{\text{bcc}}_{O}$ denote the reference state Gibbs energy for zirconium and oxygen in the bcc phase, respectively [39]. Using the formalism presented in [42], we obtain the solubility product at $T = 1273$ K, $x_{Zr}x_O = 2.0 \times 10^{-15}$, which describes the straight line depicted in Fig. 18.

Considering the thermodynamic stability of the phases, it is important to point out that the Gibbs energy of a phase depends on several state variables, which in modelling, is expressed as a function of temperature and composition [50]. From the Gibbs energy, all the state variables such as the enthalpy (H) and the chemical potential (μ) can be determined. Thus, information on experimentally determined thermodynamic quantities, like the enthalpy

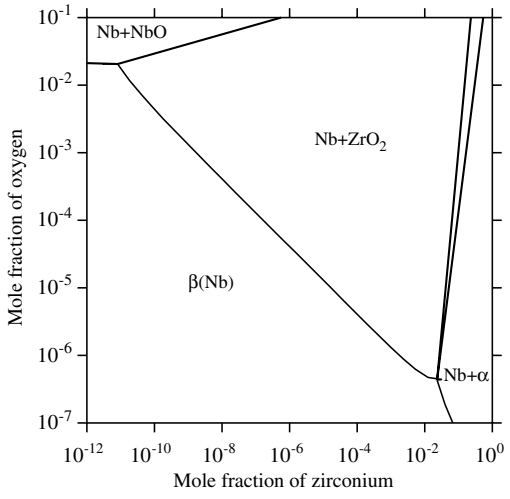

Fig. 18. The isothermal section of the Nb-rich portion of the Nb–O–Zr system at 1273 K with logarithmic axes.

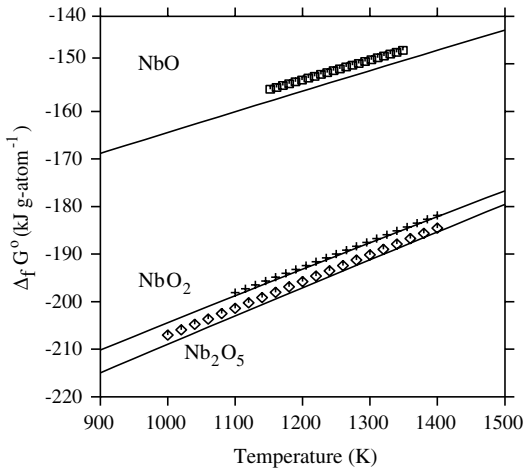

Fig. 19. The Gibbs energy of formation $\Delta_f G^0$ versus temperature, calculated (lines) and measured (symbols) for oxides: NbO, NbO_2 and Nb_2O_5.

of formation of a phase, is crucial for evaluating the phase stability. Since the details of the Nb–O system assessment had not been published [46], we calculated the thermodynamic properties of the NbO, NbO_2 and Nb_2O_5 compounds and compared our results with some of the experimental data available in literature [50–53] in order to check the stability of these oxides (Fig. 19); these are reported in Refs. [54,17]. We have also verified the calculated Nb–O phase diagram (Fig. 1) with the available experimental data [54].

To conclude, the results of our calculations show that the CALPHAD method used here describes the zirconium rich portion of the ternary Nb–O–Zr system adequately, however for the niobium rich part, the calculated results should be verified by new experiments.

Acknowledgements

We extend our thanks to Prof. Bo Sundman for discussion and guidance and Tero Manngard for help and comments. The work is supported in part by the Swedish Center for Nuclear Technology and Westinghouse Electric Sweden.

Appendix A. Definitions of terms in the compound energy formalism

The Gibbs energy per mole for a phase φ is defined as

$$G_m^{\varphi} = \sum_i \prod_s y_i^s G_i^{\mathrm{ref}} + G_m^{\mathrm{id}} + G_m^{\mathrm{ex}}, \tag{A.1}$$

$$G_m^{\mathrm{id}} = RT \sum_s \sum_i a^s y_i^s \ln(y_i^s), \tag{A.2}$$

$$G_m^{\mathrm{ex}} = \prod_i y_i^s \left(\sum_j y_j^t L_{i,j} + \sum_j \sum_k y_j^t y_k^u L_{i,j,k} + \cdots \right), \tag{A.3}$$

where G_i^{ref} is the reference Gibbs energy of the pure element i, e.g., Nb, Zr, or O in the corresponding allotropic form φ, G^{id} is the ideal Gibbs energy of mixing, G^{ex} the excess (interaction) Gibbs energy, y_j^s the site fraction of the sublattice s, R the gas constant, T the temperature, a^s the stoichiometric coefficient in the sublattice s, $L_{i,j}$ are the binary interaction parameters between elements i and j, etc. The L parameters are composition dependent and are expressed by the Redlich–Kister polynomials [55]. In terms of the site fractions, e.g., the interaction parameters between atoms A and B can be expressed in the form:

$$L_{A,B} = \sum_v L_{A,B}^v (y_A^s - y_B^s)^v, \tag{A.4}$$

where the coefficients appearing on the right-hand-side can be temperature dependent in the form $L_{A,B}^v = b_0 + b_1 T + b_2 T^2 + \cdots$, etc.

Thermodynamic equilibrium demands that the Gibbs free energy of the set of stable phases at a given T, pressure P and composition x_i is at its minimum; we write

Table B.1
Thermodynamic properties of the different phases of the Nb–O system

Parameter (J/mol)	Range (K)
$G_{NbO} = -434220.337 + 246.876204T - 42.99897T\ln(T) - 0.00443671135T^2 + 7.613485\times10^{-10}T^3 + 201346.65T^{-1}$	$298.14 < T < 2210$
$G_{NbO} = -456057.083 + 399.171599T - 62.76T\ln(T)$	$2210 < T < 6000$
$G_{NbO_2} = -817191.531 + 381.593377T - 64.17126T\ln(T) - 9.08246E-04T^2 - 4.022435\times10^{-6}T^3 + 418142.7T^{-1}$	$298.14 < T < 700$
$G_{NbO_2} = -811038.971 + 277.505525T - 47.77082T\ln(T) - 0.01985076T^2$	$700 < T < 1000$
$G_{NbO_2} = -7995222.39 + 66544.4364T - 9449.355T\ln(T) + 5.400225T^2 - 5.80159\times10^{-4}T^3 + 1.0211785\times10^{9}T^{-1}$	$1000 < T < 1300$
$G_{NbO_2} = -825146.769 + 515.555749T - 83.0524T\ln(T)$	$1300 < T < 2175$
$G_{NbO_2} = -849262.299 + 611.84916T - 94.14T\ln(T)$	$2175 < T < 6000$
$G_{Nb_2O_5} = -1942063.25 + 674.379374T - 115.742T\ln(T) - 0.0547895T^2 + 8.24945333\times10^{-6}T^3 + 534527T^{-1}$	$298.14 < T < 700$
$G_{Nb_2O_5} = -1967843.43 + 1010.19042T - 166.3182T\ln(T) - 0.010714595T^2 + 1.04697633\times10^{-6}T^3 + 2995953T^{-1}$	$700 < T < 1500$
$G_{Nb_2O_5} = -1970867.16 + 1053.49937T - 172.7281T\ln(T) - 0.0061988805T^2 + 5.181745\times10^{-7}T^3 + 2995953T^{-1}$	$1500 < T < 1785$
$G_{Nb_2O_5} = -2077756.73 + 1625.45741T - 242.2536T\ln(T)$	$1785 < T < 6000$
Liquid phase	
$G^{L}(Nb^{+2}, O^{-2}) = 2G_{NbO} + 310681.92 - 135.66551T$	$298.14 < T < 6000$
$G^{L}(NbO_2) = G_{NbO_2} + 62301 - 16.9083T$	$298.14 < T < 6000$
$G^{L}(NbO_{5/2}) = 0.5G_{Nb_2O_5} + 19682.659 - 10T$	$298.14 < T < 6000$
$L^{0,L}(Nb^{+2},O^{-2},\square) = 56277.338$	$298.14 < T < 6000$
bcc-A2 phase	
$G^{bcc}(Nb:O) = G_{Nb_2O_5} + G_{NbO} + 250000$	$298.14 < T < 6000$
$L^{0,bcc}(Nb: O, \square) = -670149 + 76.4T$	$298.14 < T < 6000$
$L^{1,bcc}(Nb: O, \square) = -354266$	$298.14 < T < 6000$
hcp-A3 metastable phase	
$G^{hcp}(Nb: O, \square) = G_{NbO} + 100000$	$298.14 < T < 6000$

$$\min_{(n^{\varphi},y)}\left\{G=\sum_{\varphi}n^{\varphi}G^{\varphi}_{m}(T,P,\mathbf{y})\right\}, \tag{A.5}$$

where n^{φ} is the amount of phase φ and $\mathbf{y}$ denotes all the site fractions in the phase. The minimization is performed subject to the following constraints:

$$1-\sum_{i}y^{s}_{i}=0;\quad n^{\varphi}\wedge y^{s}_{k}\geqslant 0. \tag{A.6}$$

In case of ionic solutions, one also has the conservation of charge, $\sum_{s,k}a^{s}v_{k}y^{s}_{k}=0$, with v_k denoting the valency of constituent k.

Appendix B. Summary of thermodynamic functions

The properties for Nb–Zr and Zr–O are well documented in Refs. [14,15], respectively and hence are not repeated here. Table B.1 lists the thermodynamic parameters, the Gibbs energies as a function of temperature, describing the Nb–O system with respect to the stable element reference H^{SER} (at temperature $T = 298.15$ K and pressure $P = 101325$ Pa). The interaction parameters are denoted by L. These results, which are input to Thermo-Calc, are based on the work of Dupin and Ansara [46,13] presented here with some minor misprint corrections and modifications of the interaction terms for the bcc-A2 phase.

References

[1] R.J. Comstock, G. Schoenberger, G.P. Sabol, in: E.R. Bradley, G.P. Sabol (Eds.), Zirconium in Nuclear Industry: Eleventh International Symposium, ASTM STP 1295, American Society for Testing and Materials, West Conshohocken, PA, USA, 1996, p. 710.
[2] J.-P. Mardon, D. Charquet, J. Senevat, in: G.P. Sabol, G.D. Moan (Eds.), Zirconium in Nuclear Industry: Twelfth International Symposium, ASTM STP 1354, American Society for Testing and Materials, West Conshohocken, PA, USA, 2000, p. 505.
[3] D.O. Northwood, X. Meng-Burany, B.W. Warr, in: C. Euken, A.M. Garde (Eds.), Zirconium in Nuclear Industry:

Ninth International Symposium, ASTM STP 1132, American Society for Testing and Materials, Philadelphia, USA, p. 156.
[4] D. Srivastava, G.K. Dey, S. Banerjee, Metall. Trans. A 26A (1995) 2707.
[5] P.V. Shebaldov, M.M. Peregud, A.V. Nikulina, Y.K. Bibilashvili, A.F. Lositski, N.V. Kuzmenko, V.I. Belov, A.E. Novoselav, in: G.P. Sabol, G.D. Moan (Eds.), Zirconium in Nuclear Industry: Twelfth International Symposium, ASTM STP 1354, American Society for Testing and Materials, West Conshohocken, PA, USA, 2000, p. 545.
[6] A.V. Nikulina, V.A. Markelov, M.M. Peregud, in: E.R. Bradley, G.P. Sabol (Eds.), Zirconium in Nuclear Industry: Eleventh International Symposium, ASTM STP 1295, American Society for Testing and Materials, West Conshohocken, PA, USA, 1996, p. 785.
[7] R.H. Titran, M. Uz, Effects of thermomechanical processing on the microstructure and mechanical properties of Nb–1Zr–1C alloys, Technical Report TM-107207, NASA, Lewes Research Center, Cleveland, Ohio, USA (1996).
[8] J.R. DiStefano, L.D. Chitwood, J. Nucl. Mater 295 (2001) 42.
[9] S.J. Zinkle, N.M. Ghoniem, Fusion Eng. Des. 51&52 (2000) 55.
[10] K. Nakai, C. Kinoshita, S. Kitajima, J. Nucl. Mater. 98 (1981) 131.
[11] M.K. Asundi, S.P. Garg, P. Mukhopdhyay, G.P. Tiwari, A. Saroja, J. Alloy Phase Diagrams 2 (1986) 141.
[12] I. Ansara (Ed.), Summary of the CALPHAD XXVIII meeting, 1999, published in Calphad, 24:183, 2000.
[13] See: <www.inpg.fr/ltpcm/base/zircobase> (1999).
[14] P. Liang, N. Dupin, S.G. Pries, H.J. Seifert, I. Ansara, H.L. Lukas, F. Aldinger, Z. Metallkunde (2001) 747.
[15] A. Fernandez-Guillermet, Z. Metallkunde 82 (1991) 478.
[16] N. Dupin, I. Ansara, C. Toffolon, C. Lemaignan, J.C. Brachet, J. Nucl. Mater. 275 (1999) 287.
[17] R.J. Perez, Thermodynamic database for zirconium alloys, Doctoral thesis, KTH, Stockholm, Sweden (2006).
[18] J.P. Abriata, J. Garces, R. Versaci, Bull. Alloy Phase Diagrams 7 (1986) 116.
[19] A. Fernandez-Guillermet, W. Huang, Z. Metallkunde 79 (1988) 88.
[20] C.E.L. Hunt, P. Niessen, J. Nucl. Mater. 35 (1970) 134.
[21] C.E.L. Hunt, P. Niessen, J. Nucl. Mater 38 (1971) 17.
[22] I.T. Bethune, C.D. Williams, J. Nucl. Mater 29 (1969) 129.
[23] D.O. Northwood, D.C. Gillies, Microstruct. Sci. 7 (1979) 123.
[24] C. Toffolon, J.-C. Brachet, C. Servant, L. Legras, D. Charquet, P. Barberis, J.-P. Mardon, in: G. Moan, P. Rudling (Eds.), Zirconium in Nuclear Industry: Thirteenth International Symposium, ASTM STP 1423, American Society for Testing and Materials, West Conshohocken, USA, 2002, p. 361.
[25] V.C. Marcotte, W.L. Larsen, J. Less-Common Met. 10 (1966) 229.
[26] A.C. Barber, P.H. Morton, High temperature refractory metals; Metal Society Conference, 34, Gordon and Breach, New York, 1996, p. 391.
[27] A.K. Shurin, V.A. Loktinov, Izv. Akd. Nauk. ESSR Metal 1 (1970) 231 (in Russian).
[28] H. Jehn, P. Ortali, Z. Metallkunde 65 (1974) 586 (in German).
[29] W.C. Wyder, M. Hoch, Trans. AIME 224 (1962) 373.
[30] K. Seta, K. Naito, J. Chem. Thermodyn. 14 (1982) 937.
[31] R. Pynn, J.D. Axe, R. Thomas, Phys. Rev. B 13 (1976) 2965.
[32] S. Yamaguchi, M. Hirabayashi, J. Appl. Crystallogr. 3 (1970) 319.
[33] M. Hirabayashi, S. Yamaguchi, T. Arai, H. Asano, S. Hashimoto, Phys. Status Solidi 23 (1974) 331.
[34] S. Hashimoto, H. Iwasaki, S. Ogawa, S. Yamaguchi, M. Hirabayashi, J. Appl. Crystallogr. 7 (1974) 67.
[35] S. Hashimoto, J. Appl. Crystallogr. 8 (1975) 243.
[36] T. Tsuji, M. Amaya, K. Naito, J. Therm. Anal. 38 (1992) 1817.
[37] T. Tsuji, M. Amaya, K. Naito, Thermochim. Acta 253 (1995) 19.
[38] B. Sundman, I. Ansara, M. Hillert, G. Inden, H.-L. Lukas, K.C.H. Kumar, Z. Metallkunde 92 (2001) 526.
[39] A.T. Dinsdale, CALPHAD 15 (1991) 317.
[40] Thermo-Calc User's Guide, Stockholm, Sweden, <www.thermocalc.se> (2003).
[41] M. Hillert, J. Alloys Compd. 320 (2001) 161.
[42] B. Sundman, J. Ågren, J. Phys. Chem. Solids 42 (1981) 297.
[43] M. Hillert, B. Jansson, B. Sundman, Z. Metallkunde 79 (1988) 81.
[44] M. Hillert, Bull. Alloy Phase Diagrams 2 (1981) 265.
[45] B. Jansson, A general method for calculating phase equilibria under different types of conditions, Technical Report. TRITA-MAC-0233, Royal Institute of Technology, Stockholm, Sweden (1984).
[46] N. Dupin, I. Ansara, System Nb–O, personal communication with N. Dupin (2005).
[47] T. Arai, M. Hirabayashi, J. Less-Common Met. 44 (1976) 291.
[48] M. Hillert, Phase Equilibria, Phase Diagrams and Phase Transformation, Cambridge University Press, Cambridge, England, 1998.
[49] V. Greiter, D. Hauck, R. Reinbach, Z. Metallkunde 57 (1966) 113 (in German).
[50] SGTE substance database, available in Thermo-Calc software.
[51] H. Inaba, T. Mima, K. Naito, J. Chem. Thermodyn. 16 (1984) 411.
[52] M.P. Marozava, L.L. Gestkina, Z. Obeshei kximij 29 (1959) 1049 (in Russian).
[53] J.F. Marucco, R. Tetot, P. Gerdanian, C. Picard, J. Solid State Chem. 18 (1976) 97 (in French).
[54] A.R. Massih, R.J. Pérez, Thermodynamic evaluation of the Nb–O system, Technical Report. PM 05-002 v2, Quantum Technologies, available from the corresponding author (2006).
[55] J.M. Prausnitz, Molecular thermodynamics of fluid-phase equilibria, Prentice-Hall, Englewood Cliffs, New Jersey, 1969.
[56] C. Vercaemer, R. Geschier, A. Clauss, J. Less Common Met. 25 (1971) 199 (in French).
[57] C. Wang, M. Zinkevich, F. Aldinger, CALPHAD 28 (2004) 281.